Nonequilibrium dynamics of four-point correlations of collective density fluctuations in a supercooled liquid

Bhaskar Sen Gupta and Shankar P. Das
School of Physical Sciences, Jawaharlal Nehru University, New Delhi 110067, India
(Received 5 December 2013; revised manuscript received 3 June 2014; published 29 July 2014)

In this paper we study the four-point correlation function χ_4 of collective density fluctuations in a nonequilibrium liquid. The equilibration is controlled by a modified stretched exponential behavior $\{\exp[-(t_w/\tau)^\beta]\}$ having the relaxation time τ dependent on the aging time t_w. Similar aging behavior has been seen experimentally in supercooled liquids. The basic equations of fluctuating nonlinear hydrodynamics are solved here numerically to obtain χ_4 for equilibrium and non equilibrium states. We also identify a dynamic length scale ξ from the equilibrated function. $\xi(T)$ grows with fall of temperature T. From a broader perspective, we demonstrate here that the characteristic signatures of dynamical heterogeneities in a supercooled liquid, observed previously in computer simulations of the dynamics of a small number of particles, are also present in the coarse grained equations of generalized hydrodynamics.

DOI: 10.1103/PhysRevE.90.012137 PACS number(s): 61.20.Lc, 64.70.pm, 64.70.qj

I. INTRODUCTION

A general feature emerging from simulations [1,2] of the particle dynamics in a liquid is that at a given instant the atomic motions in different environments in the structurally disordered system evolve differently. And yet the fluid particles constantly move and rearrange so that the distinctions between different spatial environments of the fluid are transient. Understanding this complex and evolving situation, generally termed dynamic heterogeneities [3], is facilitated through the study of the multiparticle correlation functions. The multipoint structure of the correlation function is useful in probing the cooperative nature of the dynamics since it involves incorporating the information at two different spatial points corresponding to two different times simultaneously. In a number of recent works, a dynamic length scale [4–7] depicting the strongly correlated nature of the supercooled liquid dynamics has been obtained analyzing a four-point correlation function [8]. The different types of four-point functions which have been studied in this respect involve some distinct property of the fluid [9–13] like mobility or density of a tagged particle. In the present paper we study the dynamics in terms of that of the set $\{\rho(\mathbf{x},t),\mathbf{g}(\mathbf{x},t)\}$ respectively denoting the local densities of mass and momentum of the fluid. The nature of decay in the fluctuations of these conserved fields is also the focus of the microscopic theory, termed mode coupling theory (MCT), for the slow dynamics in a supercooled liquid.

Let $\delta\rho(q,t)$ denote the Fourier transform of the density fluctuation $\delta\rho(\mathbf{x},t) = \rho(\mathbf{x},t) - \rho_0$ corresponding to wave vector q at time t. ρ_0 denotes the average density. We consider the product

$$F(q;t,t_w) \equiv \delta\rho(q,t+t_w)\delta\rho(-q,t_w) \tag{1}$$

of the respective Fourier transforms of $\delta\rho$ at times $t+t_w$ and t_w. In the following t_w will be referred to as the waiting or aging time. The normalized two-point function is defined as the noise-averaged quantity:

$$C(q,t+t_w,t_w) = \frac{\langle F(q;t,t_w)\rangle}{\langle F(q,0,t_w)\rangle}\,. \tag{2}$$

For an equilibrium state time translation invariance holds, and we have the two-point function depending only on time t, $C(q,t+t_w,t_w) \equiv \mathcal{C}(q,t)$. The long-time limit $f(q)$ of $\mathcal{C}(q,t)$ changes discontinuously at the ergodicity nonergodicity (ENE) transition of the MCT discussed above and is generally termed the nonergodicity parameter.

On the other hand the four-point function $\chi_4(q;t,t_w)$ is defined in a form normalized with respect to its initial value:

$$\chi_4(q;t,t_w) = \frac{\langle F(q;t,t_w)F(-q;t,t_w)\rangle}{|F(q;0,0)|^2}\,. \tag{3}$$

In this paper we compute the time dependent correlation function $\chi_4(q_m,t)$ involving the collective densities $\rho(\mathbf{x},t)$ at four points. Here q_m corresponds to the first maximum of structure factor. The four-point function develops a sharp peak at a time $t = t_p$ (say) and eventually decays out at larger times. The dynamic length $\xi(T)$, identified from analyzing [14] the four-point function $\chi_4(q,t_p)$, grows roughly by a factor of three over the corresponding temperature range. The quantity $\chi_0 \equiv \chi_4(0,t_p)$ grows as $\xi^{(2-\eta)}$ with the correlation length ξ with the exponent $2-\eta = 2.1$. In the nonequilibrium state without time translation invariance [15], the four-point function $\chi_4(t,t_w)$ for several different values of the waiting (aging) time t_w is seen to overlap in the α-relaxation regime. The corresponding frequency transforms $\chi_4(\omega,t_w)$ collapse on a modified Kohlrausch-Williams-Watts (MKWW) relaxation curve relaxation time $\tau(t_w)$ dependent on t_w. This is similar to the behavior seen in two-point correlations [16,17].

The dynamics of short length scale fluctuations in a dense liquid going beyond the low order mode-coupling approach has been studied by various methods. A study by Fuckizaki and Kawasaki [18] involved mapping the problem to a kinetic lattice gas-type model. In this approach density is treated as the only relevant variable, and its dynamics is studied with a discretized version of the Fokker-Planck equation in the form of a mesoscopic kinetic equation. Another nonperturbative approach [19,20] is to solve numerically the equations of fluctuating nonlinear hydrodynamics (FNH) for a small set of slow modes for the many-particle system. These studies so far were generally for two-point equilibrium correlations. We

solve the FNH equations taking into account the short wave length fluctuations and going up to long times to consider both equilibrium and nonequilibrium correlations at two- and four-point levels. The paper is organized as follows. In the next section we describe the equations of generalized hydrodynamics. In Sec. III we discuss the specific model for which these equations are solved. In Sec. IV we present the results. The paper is concluded with a short discussion of the results.

II. GENERALIZED HYDRODYNAMICS

To calculate these time correlation functions we need the dynamical equations controlling the time evolution of density fluctuations in the liquid. In the generalized hydrodynamic description, the equations of motion for the set of coarse-grained densities $\phi_i(x,t)$ are obtained in the form of Langevin equations [21]:

$$\frac{\partial \phi_i}{\partial t} = V_i[\phi] - \sum_j L^0_{ij} \frac{\delta F}{\delta \phi_j} + \theta_i. \tag{4}$$

$V_i[\phi]$ is the "streaming velocity" representing the reversible part of the equation of motion and is given by

$$V_i[\phi] = \sum_j \{\phi_i, \phi_j\} \frac{\delta F}{\delta \phi_j}, \tag{5}$$

where we have used the usual convention of repeated indices being summed over. $\{\phi_i,\phi_j\}$ is the Poisson bracket [22] between the "slow" variables and is obtained by using the definitions of the corresponding microscopic densities $\{\hat{\phi}_i\}$. The quantity $F[\phi]$ is the effective Hamiltonian governing the equilibrium averages of the fields ϕ_i at equal times, given by

$$\langle \phi_i \phi_j \rangle = \int D(\phi) e^{-\beta F[\phi]} \phi_i \phi_j / Z, \tag{6}$$

where

$$Z = \int D(\phi) e^{-\beta F[\phi]} \tag{7}$$

is the partition function, $\beta = (k_B T)^{-1}$, and $D(\phi)$ indicates a functional integral over the fields ϕ_i. The irreversible part of the dynamics is incorporated via the damping coefficient L_{ij} and the thermal noise term θ_i. The second moment of θ_i is given by

$$\langle \theta_i(\mathbf{x},t)\theta_j(\mathbf{x}'t')\rangle = 2k_B T L^0_{ij} \delta(\mathbf{x}-\mathbf{x}')\delta(t-t'). \tag{8}$$

The damping matrix L^0_{ij} is interpreted as the "bare" or local approximation for the transport coefficients, which are determined by short-range interactions.

For the compressible liquid, which is our focus here, we consider the dynamics in terms of two coarse-grained fluctuating variables, namely, the mass density $\rho(\mathbf{r},t)$ and the momentum density $g(\mathbf{r},t)$. The reversible parts V_i of the respective generalized Langevin equations (4), involving the Poisson brackets, are obtained using the microscopic expressions for the corresponding slow modes. Their calculation is standard and is described in Ref. [23]. The effective Hamiltonian or the so-called free energy functional $F[\phi]$ is a function of the coarse-grained densities $\rho(\mathbf{x})$ and $\mathbf{g}(\mathbf{x})$:

$$F[\rho,g] \equiv F_K[\rho,g] + F_U[\rho]. \tag{9}$$

The kinetic part is dependent on the momentum density

$$F_K = \int d\mathbf{x} \frac{g^2(\mathbf{x})}{2\rho(\mathbf{x})}, \tag{10}$$

and the so-called potential part is given by $F_U = F_{\rm id} + F_{\rm in}$. The ideal gas contribution $F_{\rm id}$ and the interaction part $F_{\rm in}$ are, respectively, given by

$$\beta F_{\rm id} = \frac{1}{m} \int d\mathbf{r} \rho(\mathbf{r}) \left[\ln\left(\frac{\rho(\mathbf{r})}{\rho_0}\right) - 1 \right], \tag{11}$$

$$\beta F_{\rm in} = -\frac{1}{2m^2} \int d\mathbf{x} \int d\mathbf{x}' \delta\rho(\mathbf{x}) c(x-x') \delta\rho(\mathbf{x}'). \tag{12}$$

For the interaction part $F_{\rm in}$ we have used the Ramakrishnan-Yussouff (RY) [24] form of the interaction free energy (up to second order) used in the static density functional theory. With the results stated above F is quadratic in the density fluctuations, and the probability e^{-F} of the equilibrium state is Gaussian.

The equation for mass density $\rho(\mathbf{x},t)$ is the continuity equation

$$\frac{\partial \rho}{\partial t} + \nabla \cdot \mathbf{g} = 0. \tag{13}$$

The streaming velocity for the current $g(\mathbf{x},t)$ is given by

$$V^i_g(\mathbf{x}) = -\nabla_j \left[\frac{g_i g_j}{\rho} \right] - v_0^2 [\nabla_i \rho - \rho \nabla_i f(\mathbf{r})], \tag{14}$$

where $v_0 = 1/\sqrt{\beta m}$ is the thermal speed and $f(\mathbf{r})$ is the convolution matrix,

$$f(\mathbf{r}) = m^{-1} \int d\mathbf{r}' c(\mathbf{r}-\mathbf{r}') \delta\rho(\mathbf{r}',t). \tag{15}$$

The nonlinear equations for the components of the momentum density $\mathbf{g}$ are therefore obtained in a generalized form of the Navier-Stokes equation:

$$\frac{\partial g_i}{\partial t} + \nabla_j \left[\frac{g_i g_j}{\rho} \right] + v_0^2 \{\nabla_i \rho - \rho \nabla_i f(\mathbf{r})\} + L_{ij} \frac{g_j}{\rho} = \theta_i. \tag{16}$$

Here $v_0 = 1/\sqrt{\beta m}$ denotes the thermal speed at temperature T. The second term on the LHS of Eq. (16) refers to the well-known Navier-Stokes nonlinearity and is a result of coupling of convective currents. The stochastic term in the generalized Langevin equation (16) is denoted by the noise θ_i, which is assumed to be Gaussian. The correlation of the noise is related to to the bare damping matrix L^0_{ij} through the fluctuation-dissipation relation (8). The matrix L^0_{ij} is given by

$$L^0_{ij}(\mathbf{x}) = -\eta_0 \left(\tfrac{1}{3} \nabla_i \nabla_j + \delta_{ij} \nabla^2 \right) - \zeta_0 \nabla_i \nabla_j, \tag{17}$$

where η_0 and ζ_0 are bare shear and bare bulk viscosities, respectively. L^0_{ij} is treated as an input in the calculation. We use for these bare transport coefficients Enskog-type expressions [25], which describe the short-time behavior for the liquid well. These expressions for the transport coefficients

are identified by the constructing the equations of generalized hydrodynamics from microscopic description of the fluid:

$$q^2\zeta_0(q) = \frac{2}{3t_E}[1 - j_0(q\sigma) + 2j_2(q\sigma)], \tag{18}$$

$$q^2\eta_0(q) = \frac{2}{3t_E}[1 - j_0(q\sigma) - j_2(q\sigma)]. \tag{19}$$

Here j_n is the spherical Bessel function of order n and t_E is the Enskog collision time [26].

Equations (13) and (16) form the basic set of nonlinear fluctuating hydrodynamic equations for $\{\rho,\mathbf{g}\}$. For compressible liquids the convective term [the third term of Eq. (16)] as well as the dissipative term [the fourth term of Eq. (16)] contain the $1/\rho$ nonlinearity. The density nonlinearity present in the reversible part of the equation of motion (16) has important consequences for the dynamics of the compressible liquids. This is included in the fourth term representing the pressure functional. The function $f(\mathbf{x},t)$ signifies the role of interaction between the fluid particles and is obtained in Eq. (15) as a convolution function of the direct correlation function $c(\mathbf{x})$ and the density fluctuation $\delta\rho(\mathbf{x},t)$. The slow dynamics of the MCT originates from a feedback mechanism caused by the density nonlinearities in the FNH Eq. (16). We have ignored the convective nonlinearities in Eq. (16) to focus on the role of the coupling of density fluctuations.

III. THE MODEL STUDIED

We present here the numerical scheme followed in solving the above described FNH equation. We consider here a classical system of N particles, each of mass m interacting through the Lennard-Jones (LJ) potential of characteristic length scale σ. The thermodynamic state of the fluid is described in terms of the reduced density $n_0^* = n_0\sigma^3$ and the reduced temperature $T^* = (k_BT)/\epsilon$. n_0 is the average number density of particles with $\rho_0 = mn_0$. The FNH equations are solved numerically on a cubic grid with mesh size h in three dimensions. We scale length with respect to the grid length h and time with respect to $\bar{\tau}_o \equiv h/c_0$ where c_0 is the speed of sound in the hydrodynamic limit, i.e., $c_0^2 = k_BT/[mS(0)] = v_0^2/S(0)$. In terms of the usual LJ time scale τ_0, we have $\bar{\tau} = \tau_0 S(0)/\sqrt{T^*}$. For numerical solution the conserved densities and momentum are scaled to dimensionless forms. The mass and momentum densities are, respectively, scaled as $\rho(\mathbf{x},t) \Rightarrow [(m/h^3)]n(\mathbf{x},t)$ and $\mathbf{g}(\mathbf{x},t) \Rightarrow [mc_0/h^3]\mathbf{j}(\mathbf{x},t)$. In terms of these new rescaled variables $n(\mathbf{r},t)$ and $j(\mathbf{x},t)$, the fluctuating equations have the form

$$\frac{\partial n(\mathbf{r},t)}{\partial t} + \alpha[\nabla\cdot\mathbf{j}] = 0, \tag{20}$$

$$\frac{\partial j_i(\mathbf{r},t)}{\partial t} + S(0)[\nabla_i\delta n(\mathbf{r},t) - n(\mathbf{r},t)\nabla_i\tilde{f}(\mathbf{r},t)] + \bar{L}^0_{ik}\frac{j_k(\mathbf{r},t)}{n(\mathbf{r},t)} = \bar{\theta}_i(\mathbf{r},t). \tag{21}$$

The fluctuation is defined as $\delta n(\mathbf{r},t) = n(\mathbf{r},t) - \bar{n}_0$ where $\bar{n}_0 = n_0h^3 = n^*\alpha^{-3}$ and $\alpha = h/\sigma$. The function $f(\mathbf{r},t)$ defined in Eq. (15) is obtained in the dimensionless form as $\tilde{f}(\mathbf{r},t)$:

$$\tilde{f}(\mathbf{r},t) = \int d\mathbf{r}c(\mathbf{r}-\mathbf{r}')\delta n(\mathbf{r}',t). \tag{22}$$

$\bar{\theta}_i$ is the noise reduced to dimensionless form, and its correlation is related to the bare transport matrix $\bar{L}^0_{ij}$. For the isotropic liquid $\bar{L}^0_{ij}$ is expressed in terms of two independent transport coefficients given by

$$\bar{L}^0_{ij} = (\bar{\zeta}_0 + \bar{\eta}_0/3)\delta_{ij}\nabla^2 + \bar{\eta}_0\nabla_i\nabla_j. \tag{23}$$

In the small wave number limit, $\bar{\zeta}_0$ and $\bar{\eta}_0$ are the bare bulk and shear viscosities, respectively. Since we will be applying the equations for finite wavelengths here, more generalized expressions for these quantities are necessary. We use here the Enskog-type expression [25] for this purpose, which describe the short-time behavior for the liquid quite well:

$$\bar{\zeta}_0(\mathrm{x})\mathrm{x}^2 = \nu_0[1 - j_0(\mathrm{x}) + 2j_2(\mathrm{x})], \tag{24}$$

$$\bar{\eta}_0(\mathrm{x})\mathrm{x}^2 = \nu_0[1 - j_0(\mathrm{x}) - j_2(\mathrm{x})], \tag{25}$$

where $j(\mathrm{x})$ is the spherical bessel function for the scaled wave number $\mathrm{x} = q\sigma$ and the unit $\nu_0 = (2\sigma)/(3v_0t_E)$ in terms of the Enskog collision time t_E [26].

The numerical solution scheme used here starts with an initial distribution of the fluctuating variables $n(\mathbf{r})$ and $\mathbf{j}(\mathbf{r})$ over a set of points 20^3 on a cubic lattice. The equation of motion for the density variable $n(x,t)$, i.e., the continuity equation, is linear. Let us consider the various nonlinear terms present in the equation of motion for the momentum density. First, the nonlocal integral $\tilde{f}(r,t)$ defined in Eq. (15) appears in the reversible part of the equation of motion and is evaluated as a sum of contributions from the successive shells,

$$\tilde{f}(r,t) = h^3\sum_i c(R_i)\sum_\alpha \delta n\left(R_i^\alpha,t\right), \tag{26}$$

where R_i^α for $\alpha = 1,\ldots,m_i$, respectively, denote radii vectors of the m_i lattice points in the ith spherical shell of radius R_i. Second, the $1/n(\mathbf{x},t)$ nonlinearity in the dissipative term of the momentum equation is computed by replacing the density field in the denominator with the $n(\mathbf{x})$ averaged over a length scale close to σ around the corresponding point $\mathbf{r}$. Finally we ignore the convective nonlinearity in the present calculation and focus on the role of the pressure nonlinearity in producing the slow dynamics.

To avoid the spurious instability due to the density becoming negative on a grid point in the numerical solution scheme, we adopt a coarse-graining scheme [27] in which the density $n(\mathbf{x},t)$ on the grid is redefined at each step of the numerical integration.

Equations (13)–(16) of FNH are solved numerically on a cubic lattice of size 20 with a grid length h. Two inputs are required here. First is the direct correlation function $c(r)$ related to the structure of the liquid [28]. Second, the bare transport coefficients L^0_{ij} defining the noise correlations are chosen such that the corresponding short-time dynamics agrees with computer simulation data. For displaying the figures time is scaled with $\tau_0 = (m\sigma^2/\epsilon)^{\frac{1}{2}}$ and length with lattice constant h. Starting from an uniform configuration of

density and momentum density on the grid of points, we solve the equations of motion progressively in time and the results for the density fluctuations are saved in selected time bins. The whole array consisting of the density fluctuations $n(\mathbf{x},t)$ at different lattice points $\mathbf{x}$ are then transformed using fast Fourier transform subroutines and stored as $n(\mathbf{k},t)$ in selected time bins. These data repeated over different sets of initial conditions are averaged to obtain the correlation functions. The density fluctuations are saved in selected time bins. A whole array consisting of the density fluctuations $\rho(\mathbf{x},t)$ on the cubic lattice $\mathbf{x}$ are transformed using fast Fourier transform subroutines. From this data the two-point and four-point correlation functions are respectively obtained. Several runs for the dynamic evolution of the system driven by the noise is considered. Equilibrium is inferred when time translational invariance of the correlation function is observed; i.e., the two time correlation function $C(t_w,t+t_w)$ depends on t only. This is attained at increasingly larger t_w as the liquid is further supercooled.

IV. RESULTS

We equilibrated the system at average density $\rho_0^* = 1.10$ and temperatures, respectively, at $T^* = 1.0$, 0.8, 0.7, 0.6, and 0.5. For even lower temperatures $T^* = 0.4$ the system does not equilibrate within the maximum time limit of computation time. The ratio of the two characteristic lengths $\sigma/h = 4.6$ is kept fixed. The data for $\rho(\mathbf{x},t)$ and $\mathbf{g}(\mathbf{x},t)$ at each of the grid points are stored for times at equal intervals extending up to a maximum time $t_{\max}$ depending on the temperature T^*. For $T^* = 0.6$ we have $t_{\max}$ $(2000\tau_0)$. To study the equilibrium correlation functions, we consider large enough initial times t_w. Figure 1 displays the time dependence of the four-point function $\chi_4(t)$ obtained by evaluating the RHS of Eq. (3) for $q = q_m$. The time axis is plotted on the logarithm to the base 10. From the same data for the $\rho(\mathbf{x},t)$ the two-point equilibrium correlation function $C(t+t_w,t_w) \equiv \mathcal{C}(t)$ is also obtained, and the time dependence is displayed in Fig. 2 for

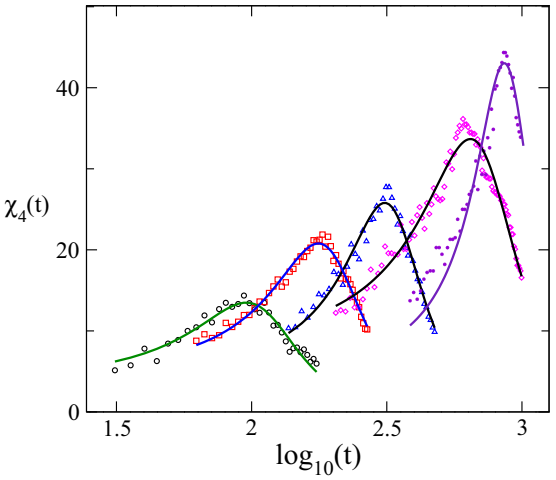

FIG. 1. (Color online) The normalized four-point functions $\chi_4(t)$ at $q = q_m$ vs time t at $n_0^* = 1.10$ and $T^* = 1.0$ (circles), 0.8 (squares), 0.7 (triangles), 0.6 (diamonds), 0.5 (stars). Solid lines are the best fit curves of Lorentzian form.

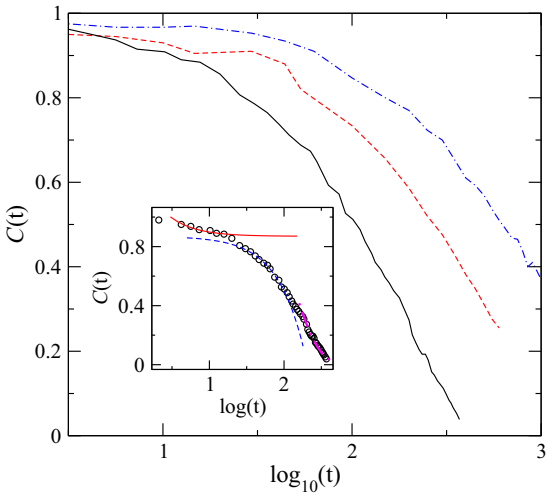

FIG. 2. (Color online) The normalized two-point function $C(t)$ at $n_0^* = 1.10$ and $T^* = 0.8$ (solid), 0.7 (dashed), and 0.6 (dashed-dotted). In the inset the solid and dashed curves indicate the respective power law fits predicted in MCT for $T^* = 0.8$.

temperatures $T = 0.8$,0.7, and 0.6. The two-point function $\mathcal{C}(t)$ reaches a small plateau value $f_c = 0.87$ at $T^* = 0.8$. Following the predictions of MCT [29] the exponents a and b corresponding to the power law and subsequent von Schneider relaxation are 1.27 and 1.18, respectively. These values are obtained from simply fitting the equilibrated time correlation function to the two respective power law forms. Thus we see some signatures of the MCT-type power law relaxation here though the exponents are not related by the standard equation of the one-loop MCT in terms of the gamma functions. The corresponding temperature T_c is obtained from the nonzero solution of the integral equations (for the NEPs) obtained in the one-loop model. With the input static structure factor for the liquid, which is same as that used in the FNH equations, the T_c obtained from solution of the integral equations of MCT is in fact much higher and is close to the temperatures studied here. In the nonperturbative calculation quantitative agreement with the one-loop MCT is absent. The functional form for the final decay of the two-point density correlation function is a stretched exponential function $\exp[-(t/\tau)^\beta]$.

For the four-point function χ_4 shown in Fig. 1 the peak height χ^P is attained at $t = t_p$, which grows with supercooling indicating the growth of amorphous cluster size. We obtain $\chi^P \sim (T - T_o)^{-1.2}$ with $T_o = 0.2$ as shown in Fig. 3. The growth of t_p observed with fall of T is not as strong as that of the α-relaxation time τ_α over the same temperature change. The inset of Fig. 3 displays the dependence $\chi^P \sim t_p^\mu$ with the exponent $\mu = 0.47$. In Fig. 4 we show how the α-relaxation time grows with lowering of the temperature. By fitting the α-relaxation time τ_α to a power law divergence form we obtain $T_c = 0.4$ in the present case [17] of a one-component LJ system.

The four-point correlation function $\chi_4(q,t)$ obtained above is further analyzed to obtain the dynamic correlation length ξ. In Fig. 5 we show the scaling of the peak height $\chi_4(q,t_p) \equiv \chi^P(q)$ for different values of wave vector q using the Ornstein-Zernike form, which includes the $O(q^4)$ [10,30]

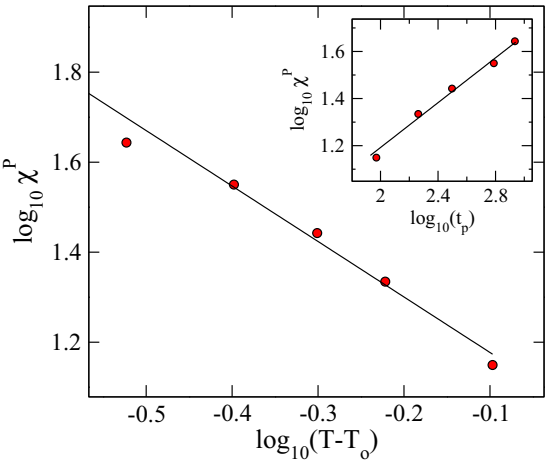

FIG. 3. (Color online) The peak χ^P of $\chi_4(t)$ at $t = t_p$ appear to diverge around $T_o = 0.2$ with exponent $\alpha = 1.21$. Inset shows $\chi^P \sim t_p^{\mu}$ behavior with the exponent $\mu = 0.47$.

contribution. From the wave vector-dependent data at a fixed T, the correlation length $\xi(T)$ is obtained. Figure 5(a) shows in the $\xi(T)$ versus T plot that the dynamic correlation length does not diverge around the so-called MCT transition temperature T_c. The length $\xi(T)$ increases by only a factor of 3, which is close to corresponding results seen in MD simulation of a binary LJ mixture [9] over a similar temperature range. In Figure 5(b) a plot of the peak height $\chi_0 \equiv \chi_4(q = 0, T)$ versus the correlation length ξ shows that $\chi_0 \sim \xi^{(2-\eta)}$ with $2 - \eta = 2.1$. The corresponding value of $(2 - \eta)$ from simulation of Ref. [14] is 2.2–2.4. With a simplified form of the MCT model in terms of density only, summing a class of ladder diagrams for the four-point functions [31], however, obtains a different prediction $2 - \eta = 4$. The two- and the four-point correlation functions are computed here using the same density fluctuation data obtained from the solution of the FNH equations. From the two-point correlation $C(t)$ the relaxation time $\tau_\alpha(T)$ is obtained, while the the dynamic length scale $\xi(T)$ follows from the study of the four-point functions $\chi_4(t)$. The temperature

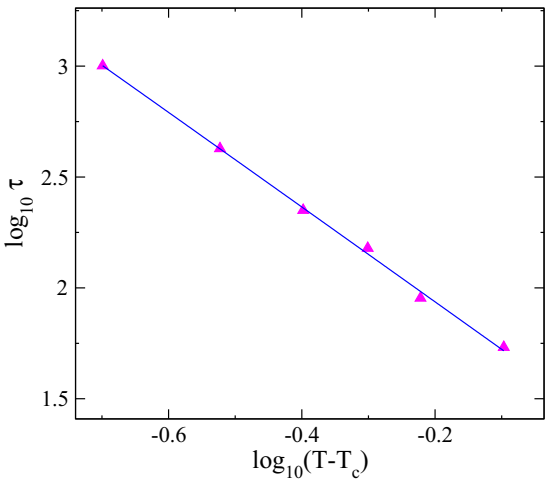

FIG. 4. (Color online) The α-relaxation time τ_α vs T. The fit shows a power law divergence around $T_c = 0.4$.

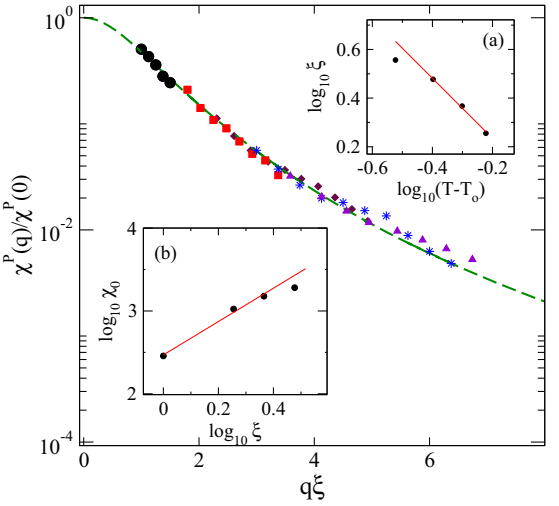

FIG. 5. (Color online) The normalized $\chi^P(q)/\chi^P(0)$ for density $n_0^* = 1.10$ and different temperatures $T^* = 1.0$ (circles), 0.8 (squares), 0.7 (diamonds), 0.6 (triangles), and 0.5 (stars) plotted with corresponding $q\xi(T)$. Dashed line is the best fit to an Ornstein-Zernike form (see text). Inset (a) divergence ξ around the $T_o = 0.2$ and exponent 1.4; (b) $\chi^P(q = 0) \equiv \chi_0 \sim \xi^{(2-\eta)}$ with $2 - \eta = 2.1$.

dependence of the different characteristic properties τ and ξ differs qualitatively. The relaxation time $\tau_\alpha(T)$ tends to diverge around a relatively higher temperature (T_c), while the growth of $\xi(T)$ does not show any change of behavior around T_c, but increases around a lower temperature.

To focus on the nonequilibrium dynamics we study the waiting time (t_w) dependence of the four-point function $\chi_4(t, t_w)$ defined in Eq. (3) for $t_w = 200, 400, 600, 800, 1000$. The $\chi_4(t)$ in each case grows to a peak of height $\chi^P(t_w)$ (say) at time $t = t_p(t_w)$. This is shown in Fig. 6. The peak time t_p grows with t_w and reaches a maximum at an intermediate t_w before equilibrating for even longer waiting times as

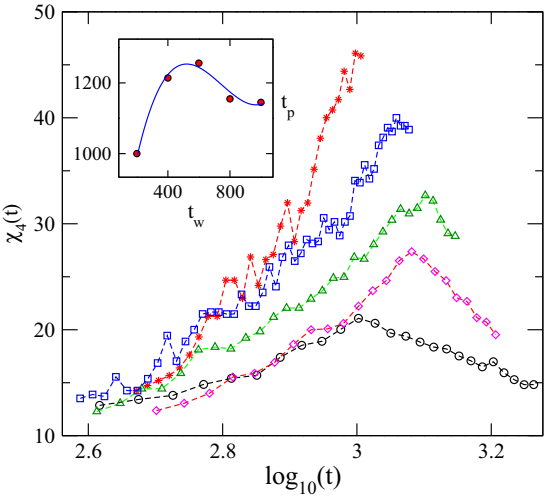

FIG. 6. (Color online) The nonequilibrium $\chi_4(t, t_w)$ vs t for different values of the waiting time t_w= 200 (circles), 400 (diamonds), 600 (triangles), 800 (squares), and 1000 (stars) corresponding to $T^* = 0.4$ and $n_0^* = 1.10$. Inset: peak time t_p vs t_w.

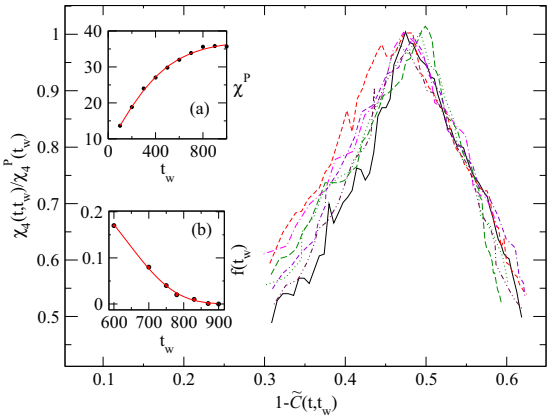

FIG. 7. (Color online) At $T^* = 0.6$ and $n_0^* = 1.10$, parametric plot of normalized $\chi_4(t,t_w)/\chi^P(t_w)$ vs $1-\tilde{C}(t,t_w)$ (see text). Equilibration with waiting time t_w: Inset (a) the peak value χ^P; (b) $f(t_w)$ (defined in text).

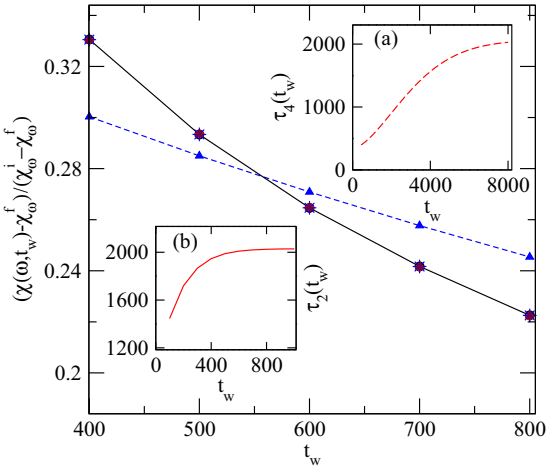

FIG. 8. (Color online) Data collapse (solid line) on the scaling function $g(t_w)$ (defined in the text) vs t_w corresponding to four different frequencies $\omega\tau_0 = 0.0001$ (circle), 0.0005 (diamond), 0.001 (triangle), and 0.01 (star) at $T^* = 0.6$ and $n_0^* = 1.10$. Scaling function corresponding to two-point functions (dashed line). The t_w dependence of relaxation times of MKWW scaling functions: Inset (a) $\tau_4(t_w)$ for four-point functions; (b) $\tau_2(t_w)$ for two-point functions.

shown in the inset of Fig. 6. The peak height χ^P of the corresponding $\chi_4(t,t_w)$ increases with t_w, signifying growing dynamic correlation. A parametric plot of $\chi_4(t,t_w)$ versus $C(t,t_w)$ is useful for understanding the evolution of the two- and four-point correlations in the nonequilibrium system. The α-relaxation parts of the $\chi_4(t,t_w)$ curves for different t_w overlap [32] with the corresponding two-point function $C(t,t_w)$ being shifted by a t-independent part $f(t_w)$. We plot in Fig. 7 the $\chi_4(t,t_w)$ with respect to the quantity

$$\tilde{C}(t,t_w) = C(t,t_w) + f(t_w). \tag{27}$$

The part $f(t_w)$ decays to zero as equilibrium is reached as shown in the inset of Fig. 7. We transform the $\chi_4(t,t_w)$ with respect to time t to obtain $\chi_4(\omega,t_w)$ corresponding to frequencies given by $\omega\tau_0 = 0.0001, 0.0005, 0.001$, and 0.01. The data for all ω values fit well to the form

$$\chi(\omega,t_w) = [\chi^i(\omega) - \chi^f(\omega)]g(t_w) + \chi^f(\omega), \tag{28}$$

where $\chi^i(\omega)$ and $\chi^f(\omega)$, respectively, denote the initial and final values of the χ_4 at the corresponding ω. The relaxation function $g(t_w)$ has limiting values 1 and 0, respectively, as $t_w \to 0$ and ∞. In the main panel of Fig. 8 we show how the data for all frequencies at $T^* = 0.6$ collapse on a single curve (solid line) giving a *frequency-independent* $g(t_w)$. The inset displays the t_w dependence of the relaxation time $\tau(t_w)$ characterizing the MKWW form of $g(t_w)$. The relaxation time $\tau(t_w)$ increases with t_w, implying that aging slows at the longer waiting time t_w. This is similar to the observed behavior [16,17] with respect to the two-point functions (dashed line in the main figure) obtained from experimental data. However for the four-point functions the time t_w to reach saturation in $\tau(t_w)$ is much longer than that for two-point case and is shown in the inset of Fig. 8.

V. DISCUSSION

The method followed in the present work has its roots in Refs. [18,19] used in dynamic density functional approach. We have demonstrated here that the appearance of a growing peak in the four-point correlation function $\chi_4(t)$ is a general feature of the dynamics of supercooled liquid, and it follows from the basic equations of generalized hydrodynamics signifying conservation laws. This holds even if the two-step process (power law and von Schneider law) predicted in the simple MCT [29] is not very clearly visible in the relaxation of two-point correlation function $\mathcal{C}(t)$. Indeed, for the simple LJ system considered here $\mathcal{C}(t)$, shown in the inset of Fig. 1, hardly freezes on any plateau so as to justify a two-step relaxation process. The same density fluctuation data obtain the prominent peak in the four-point function $\chi_4(t)$ growing with fall of temperature.

The choice of the grid size of $h \approx 0.2\sigma$ allows taking into account fluctuations up to short length scales. However, this makes the size of the box small (about 4.3σ). For calculating correlations near the peak of the structure factor, taking a larger sized box than what has been used here does not influence the results strongly [33]. It should be noted also that the dynamic correlation length found in this case as well as in the simulations [9] are less than 10σ and not largely affected by relatively small size of the box. We also maintain the periodic boundary conditions to reduce finite size effects.

A key observation from our computation of the two- and the four-point correlation functions, using the same density fluctuation data is that the temperature dependence of the relaxation time $\tau_\alpha(T)$ [obtained from $\mathcal{C}(t)$] differs qualitatively from that of the dynamic length scale $\xi(T)$ [obtained from $\chi_4(t)$]. We observe that the $\tau_\alpha(T)$ tends to diverge around a relatively higher temperature (T_c) while the growth of $\xi(T)$ appears at best to be linked to an underlying transition at T_g or T_K [34] and not to the MCT transition at T_c. At a quantitative level, however, the results for χ_4 obtained from the present work differ from the predictions of a simplified MCT model, which involves an ideal ENE transition. This is perhaps not unexpected given the fact that the oversimplified treatment of MCT gets modified in the extended MCT [23] when the implications of the $1/\rho$ nonlinearities are taken into account.

From a wider perspective what is more relevant [35] is that the general features of dynamical heterogeneities follow from the basic equations of FNH, which are also the starting point of the MCT.

ACKNOWLEDGMENTS

B.S. acknowledges CSIR India for financial support. S.P.D. acknowledges Project No. 2011/37P/47/BRNS of DAE for financial support.

[1] R. Yamamoto and A. Onuki, J. Phys. Soc. Jpn. **66**, 2545 (1997).
[2] M. M. Hurley and P. Harrowell, Phys. Rev. E **52**, 1694 (1995).
[3] M. D. Ediger, Annu. Rev. Phys. Chem. **51**, 99 (2000).
[4] S. Franz and G. Parisi, J. Phys. Cond. Matt. **12**, 6335 (2000).
[5] C. Donati, S. Franz, G. Parisi, S. C. Glotzer, J. Non-Cryst. Solids **307-310**, 215 (2002).
[6] L. Berthier, G. Biroli, J.-P. Bouchaud, L. Cipelletti, D. El Masri, D. L'Hôte, F. Ladieu, and M. Pierno, Science **310**, 1797 (2005).
[7] G. Szamel, Phys. Rev. Lett. **101**, 205701 (2008).
[8] C. Dasgupta, A. V. Indrani, S. Ramaswamy, and M. K. Phani, Europhys. Lett. **15**, 307 (1991).
[9] L. Berthier, G. Biroli, J.-P. Bouchaud, W. Kob, K. Miyazaki, and D. Reichman, J. Chem. Phys. **126**, 184503 (2007); **126**, 184504 (2007).
[10] R. S. L. Stein and H. C. Andersen, Phys. Rev. Lett. **101**, 267802 (2008).
[11] G. Biroli, J.-P. Bouchaud, K. Miyazaki, and D. R. Reichman, Phys. Rev. Lett. **97**, 195701 (2006).
[12] G. Szamel and E. Flenner, Phys. Rev. E **74**, 021507 (2006).
[13] T. Bauer, P. Lunkenheimer, and A. Loidl, Phys. Rev. Lett. **111**, 225702 (2013).
[14] S. Karmakar, C. Dasgupta, and S. Sastry, Phys. Rev. Lett. **105**, 015701 (2010).
[15] W. Kob and J.-L. Barrat, Phys. Rev. Lett. **78**, 4581 (1997).
[16] P. Lunkenheimer, R. Wehn, U. Schneider, and A. Loidl, Phys. Rev. Lett. **95**, 055702 (2005).
[17] B. S. Gupta and S. P. Das, J. Chem. Phys. **136**, 154506 (2012).
[18] K. Fuchizaki and K. Kawasaki, J. Phys. Cond. Mat. **14**, 12203 (2002).
[19] L. M. Lust, O. T. Valls, and C. Dasgupta, Phys. Rev E. **48**, 1787 (1993).
[20] O. T. Valls and G. F. Mazenko, Phys. Rev A. **46**, 7756 (1992).
[21] G. F. Mazenko, *Nonequilibrium Statistical Mechanics* (Wiley, New York, 2006).
[22] I. E. Dzyaloshinskii and G. E. Volovick, Annals. Math. **61**, 555 (1980).
[23] S. P. Das and G. F. Mazenko, Phys. Rev. A **34**, 2265 (1986).
[24] T. V. Ramakrishnan and M. Yussouff, Phys. Rev. B **19**, 2775 (1979).
[25] S. P. Das and J. W. Dufty, Phys. Rev. A **46**, 6371 (1992).
[26] J. Boon, and S. Yip, 1991, *Molecular Hydrodynamics* (Dover, New York, 1991).
[27] B. S. Gupta, S. P. Das, and J.-L. Barrat, Phys. Rev. E **83**, 041506 (2011).
[28] D. M. Due and A. D. J. Haymet, J. Chem. Phys. **103**, 2625 (1995).
[29] S. P. Das, Rev. Mod. Phys. Rev. **76**, 785 (2004).
[30] S. Karmakar, C. Dasgupta, and S. Sastry, Proc. Natl. Acad. Sci. U.S.A. **106**, 3675 (2009).
[31] G. Biroli, and J.-P. Bouchaud, Europhys. Lett. **67**, 21 (2004).
[32] S. K. Nandi and S. Ramaswamy, Phys. Rev. Lett. **109**, 115702 (2012); arXiv:1309.2389.
[33] B. S. Gupta and S. P. Das, Int. J. Mod. Phys. B **26**, 1250146 (2012).
[34] G. Adam and J. H. Gibbs, J. Chem. Phys. **43**, 139 (1965).
[35] L. Berthier and J. P. Garrahan, Phys. Rev. E **68**, 041201 (2003).